Journal of Materials Chemistry C

Accepted Manuscript

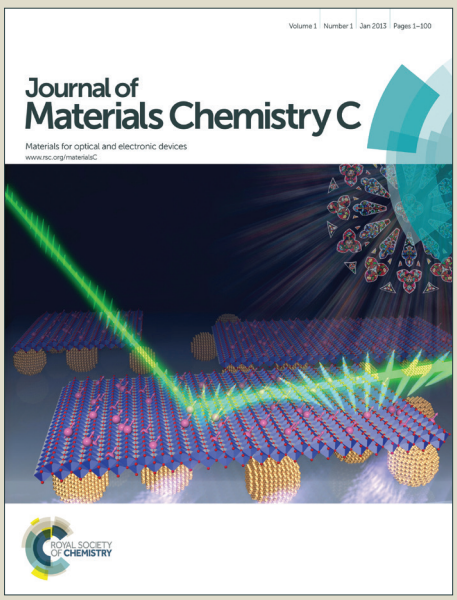

ROYAL SOCIETY OF CHEMISTRY

www.rsc.org/materialsC

Journal of Materials Chemistry C

RSCPublishing

ARTICLE

Enhanced Light-Matter Interaction of Graphene-Gold Nanoparticles Hybrid Films for High-Performance SERS Detection

Cite this: DOI: 10.1039/xoxxooooox

Received ooth January 2012,
Accepted ooth January 2012

DOI: 10.1039/xoxxooooox

www.rsc.org/

Yuanxin Du,[a] Yuan Zhao,[a] Yan Qu,[b] Chia-Hao Chen,[c] Chieh-Ming Chen,[d] Cheng-Hao Chuang,[d] and Yanwu Zhu[a]*

By simply coating graphene films on Au nanoparticles, the optical properties of the hybrid films are investigated. It is found that the coverage of a monolayer graphene film leads to a decreased transmittance of up to 15.8% in the visible range, much higher than the 2.3% transmittance loss for intrinsic graphene. At the same time, the plasmonic resonance of the hybrid films experiences a red-shift in resonant frequency and a broadening in the transmission dip. By means of finite element simulations, these observations are attributed to the strong light-matter interaction at the interface between graphene and Au nanoparticles, as indicated by the increased absorption cross section and higher electric field intensity. The electron transfer between graphene and Au nanoparticles is confirmed by high resolution X-ray photoelectron spectroscopy studies. Furthermore, the enhanced electromagnetic hot spots at the interface between graphene and Au nanoparticles make such graphene-Au nanoparticles hybrid films cost-effective and high-performance surface-enhanced Raman scattering substrates for detecting organic molecules such as rhodamine-6G, for which an enhancement factor of ~10^7 is achieved.

1. Introduction

Graphene, a flat monolayer of sp^2 carbon atoms in a hexagonal lattice configuration,[1] continues to attract intensive interest because of its excellent optical[2,3] and electronic properties,[4,5] which make graphene promising for applications in photonic or optoelectronic devices, such as photodetectors,[6] phototransistors[7] and optical modulators.[8] The light absorption of pristine graphene maintains at a level of 2.3%, independent on wavelength in the visible and near infrared range, which has triggered a mass of research using graphene as transparent conducting films.[9] However, such a weak and wavelength-independent absorption in the visible range may cause substantial restrictions and challenges for electro-optical and all-optical applications where controlling light absorption at specific wavelengths is needed.[10,11] On the other hand, due to the unique and tunable optical properties of localized surface plasmons, metallic plasmonic nanostructures have been investigated for decades and are believed to be one of the most promising candidates for applications in photodetectors,[12] photo-diagnostics and photothermal therapy,[13,14] surface-enhanced Raman scattering (SERS)[15] and molecular imaging and sensing.[16,17] Thus combining graphene and conventional metallic plasmonic nanostructures has been an effective way to enhance the light-matter interaction in visible wavelengths, which could excite potential applications in many fields. For example, hybrid films of graphene and plasmonic metallic structures have been utilized in photovoltaic devices[18] or high-speed optical communications[12] to simultaneously enhance the incident light absorption and the carrier separation efficiency which mainly relies on the high carrier mobility in graphene. Due to the excellent bio-compatibility and chemical-stability of graphene, considerable efforts have been devoted to graphene-based SERS sensors towards future techniques for the identification and detection of chemical and biological species in a label-free environment.[19,20]

In graphene-based SERS configurations, graphene plays multiple roles such as a fluorescence quencher, an additional chemical enhancer, a molecule enricher and a building block as a flat surface substrate by the virtue of its two-dimensional (2D) structure.[21] It has been accepted that the enhancement in the local electromagnetic field in the hybrids mainly contributes to SERS signals of adsorbates, in addition to graphene-related weak chemical enhancement.[22] In most graphene-based SERS works metal nanostructures were loaded on graphene in liquid systems.[19,23,24] Since the direct contact between molecules to be detected and bare metal nanoparticles is inevitable in the liquid-based graphene-metal hybrids, the SERS detection in liquids would have to suffer the following disadvantages: (1) ambiguous mechanism explanations such as hot spots effect caused by nanoparticle aggregates, chemical adsorption-induced vibrations, charge transfer between metal and molecules; (2) a false positive detection due to the interference of impurities in complex solution system; (3) unfavorable

disturbances such as photo-induced damages and metal-catalyzed side reactions. Recently, hybrid films consisting of graphene layers and metallic nanostructures have been developed en route to lower detection limits and facile detection realization. For example, Zhu *et al.* transferred graphene on Au nanovoid arrays made by sphere templates[25] and Wang *et al.* fabricated graphene/Au nano-pyramids hybrids via standard lithography[26] for SERS detection of rhodamine-6G (R6G) with enhancement factors of 10^3 and 10^{10}, respectively. A simpler and cost-effective fabrication of graphene-metal hybrids SERS sensors is desired for a reliable and potable detection with high accuracy and good stability.

In present study, we fabricated graphene-coated plasmonic nanostructures by simply coating graphene layers onto Au nanoparticles (NPs) to detect R6G with a large enhancement factor of ~10^7. From such graphene-nanoparticles hybrid films, we observed a dramatic enhancement of the light-matter interaction, enabling a decrease in the light transmittance of up to 15.8% and significant plasmon resonance frequency red-shifts. The effects of size and density of Au NPs, and number of graphene layers were investigated. The experimental observations were further explained by numerical simulations based on finite element method (FEM) theory. Due to the increased electromagnetic field and the intrinsic chemical enhancement of graphene, the hybrid films have been found an excellent SERS substrate.

2. Materials and methods

2.1 Chemicals and materials

Chloroauric acid ($HAuCl_4 \cdot 4H_2O$, 99.9%), sodium citrate ($Na_3C_6H_5O_7 \cdot 2H_2O$, 99.8%), hydrogen peroxide (H_2O_2, 30%), sulfuric acid (H_2SO_4, 98%), ethanol, acetone, were purchased from Sinopharm Chemical Reagent Co., Ltd. (Shanghai, China). 3-aminopropyltriethoxysilane (3-APTS) and rhodamine-6G (R6G) were obtained from Sigma-Aldrich. All of these reagents were used without further purification. Ultrapure water (18.2 MΩ·cm) was produced using a water purification system (MERCK Millipore Direct-Q3).

2.2 Synthesis and deposition of Au nanoparticles

Au NPs were prepared by the chemical reduction of chloroauric acid with sodium citrate. The size of Au NPs was tuned by changing the volume of sodium citrate solution.[27] To deposit Au NPs, various substrates were treated with H_2SO_4/H_2O_2 (3:1 v/v) at 80 °C for 30 min to derive a hydroxyl surface. Then the substrates were immersed in 10% 3-APTS ethanol solution for 2h and fully modified with $–NH_2$ end groups. Unbound redundant 3-APTS monomers were removed by being rinsed profusely with ethanol. The 3-APTS-modified substrates were immersed into colloidal Au NPs then rinsed profusely with ultrapure water and dried in air, resulting in the formation of a layer of Au NPs on the substrate surface. The cover density of Au NPs was controlled by varying the immersion duration in the Au NPs colloidal suspension.[27]

2.3 CVD-grown monolayer graphene transfer

Graphene was synthesized by atmospheric pressure chemical vapor deposition (CVD) at 1000 °C on copper foils with methane as carbon source.[28] Subsequently, the graphene films were transferred onto the Au NPs coated substrates by using the thermal release tape method.[29]

2.4 Characterization and instruments

Scanning electron microscopy (SEM, JSM-6700F) and atomic force microscopy (AFM, DI Innova) were used to characterize the morphology of Au NPs deposited on substrates, before and after graphene transfer. Transmission electron microscopy (TEM, JEOL 2010) was utilized to characterize the size and structure of Au NPs. UV-vis absorbance and transmittance spectra were recorded with a Shimadzu Solid 3700 spectrometer. X-ray photoelectron spectroscopy (XPS) was utilized to determine the core-level binding energy (BE) profile of elements. The XPS spectra of graphene/Au/ITO and Au/ITO samples were measured with photon energy of 380 eV in the beamline 09A1 at National Synchrotron Radiation Research Center (NSRRC), Taiwan. The precise energy resolution (< 0.10 eV) was achieved by combination of the spherical grating monochromator (SGM) with a line density of 400 1/mm and PHI electron energy analyzer (Model 1600/3057) with a pass energy of 5.85 eV. After being calibrated with XPS spectra of standard HOPG and Au samples, the photoelectron spectra were subtracted with the background intensity around the pre-edge range and were normalized to the background intensity around the far-edge range to avoid different photon flux effects. Raman measurements were conducted with a Renishaw inVia Raman Microscope equipped with a CCD detector with an excitation wavelength of 532 nm. For SERS detection, 2 μL aliquots of R6G in ethanol with different concentrations were dropped and dispersed onto as-prepared substrates and dried in air. The Raman spectra were recorded using a 532 nm laser with 0.5 mW power and a 50× objective for all samples. The integral time was 1 s with accumulation of 5 rounds.

2.5 Finite element numerical simulation method

To rationalize the effect of the graphene on the plasmonic properties of the hybrid films, FEM numerical electromagnetic simulations have been performed using Comsol Multiphysics (COMSOL 4.3a). In the simulations, Au hemispheres with a diameter of 30 nm, with or without a layer of conformed graphene, was placed on the surface of a semi-infinite glass substrate. A plane light-wave was launched perpendicular to the substrate with a single polarized electrical field, E_y. The simulation area was 60 nm×60 nm in the horizontal dimension, and the computational domain was considered as a single unit cell. Perfectly matched layer (PML) absorbing boundary conditions were adopted in the boundary. The absorption cross section was calculated using

$$P_{abs} = \frac{\pi c \varepsilon_0}{\lambda} \int \varepsilon''(\lambda) |E(\lambda)|^2 dV \quad , (2)$$

where λ is the incident wavelength; c is the speed of light; ε_0 is the vacuum permittivity; $\varepsilon''(\lambda)$ is the imaginary of the

dielectric constant and E is the electric field, the integral is taken over its volume. The dielectric constant of Au was calculated using Drude model.[30] The refractive index of graphene in the visible range is governed by $n_g=3.0+C(\lambda_0/3)i$, where the constant $C\approx5.446\ \mu m^{-1}$ is implied by the opacity measurement by Nair *et al.*,[31] and λ_0 is the vacuum wavelength. The thickness of monolayer graphene was set as 0.5 nm; multiple graphene layers were considered as homogenous stacking of monolayer graphene.

3. Results and discussion

3.1 Fabrication and characterizations of the graphene-Au nanoparticles hybrid films

The fabrication procedure of the graphene-coated Au NPs is schematically illustrated in Fig. 1a. For the deposition of Au NPs, 3-aminopropyltriethoxysilane (3-APTS) was first linked onto the surface of the chemically treated substrates to form a monolayer of APTS with $-NH_2$ end groups. When the substrate was immersed in the Au NPs colloid suspension, the Au NPs were attached onto the surface by the interaction between particles and $-NH_2$ end groups, resulting in a uniform sub-monolayer deposition of Au NPs on the substrate, as shown in the scanning electron microscopy (SEM) and atomic force microscopy (AFM) images in Fig. 1b and d, respectively. The as-synthesized Au NPs have an average size of ~30 nm, as confirmed by transmission electron microscopy (TEM) (inset of Fig. 1b); other two types of Au NPs with average sizes of ~15 nm and ~45 nm were also fabricated (see TEM images in Fig. S1†). By changing the immersing duration, the cover density for the ~30 nm Au NPs has been tuned as about 69, 122, 221, 343 and 408 particles per μm^2 (No./μm^2) (see SEM images in Fig. S3†). The ratio of Au NPs in aggregates was calculated and shown in Table S1†. We can see that the ratio falls in between 13.22-14.38 % for the cover density of from ~69 to ~343 No./μm^2, while the highest cover density of ~408 No./μm^2 led to a higher aggregation ratio of 19.63%.

Graphene grown by chemical vapor deposition (CVD) was transferred onto Au NPs on various substrates. Fig. 1c shows the typical SEM image of the graphene-Au NPs hybrid films. The area with graphene cracks was selected and zoomed to identify the existence of graphene by contrast. Due to the enhanced conductivity, graphene covered region has a darker contrast in the second electron imaging mode. The SEM image in Fig. S2a† further reveals the successful transfer of large-area graphene on top of Au NPs. The Raman spectrum in the inset of Fig. 1c confirms the monolayer nature of the graphene transferred on Au NPs. The intensity ratio of 2D/G is 3.16 and the symmetric 2D band is centered at ~2680 cm^{-1} with a full width at half maximum of ~32 cm^{-1}, which are typical features of monolayer graphene. The absence of detectable D peak suggests the absence of microscopic disorder in graphene after being transferred on Au NPs. The Raman signals from monolayer graphene (Fig. S2b†) placed on the top of Au NPs have been dramatically enhanced by the plasmonic nanostructure as reported by others.[25] The graphene cut from the same growth was transferred onto 300 nm SiO_2/Si or quartz substrates to further confirm the large-area completeness and uniformity of the monolayer graphene using optical microscope or transmittance spectrum, as shown in Fig. S2c† and S2d†, respectively.

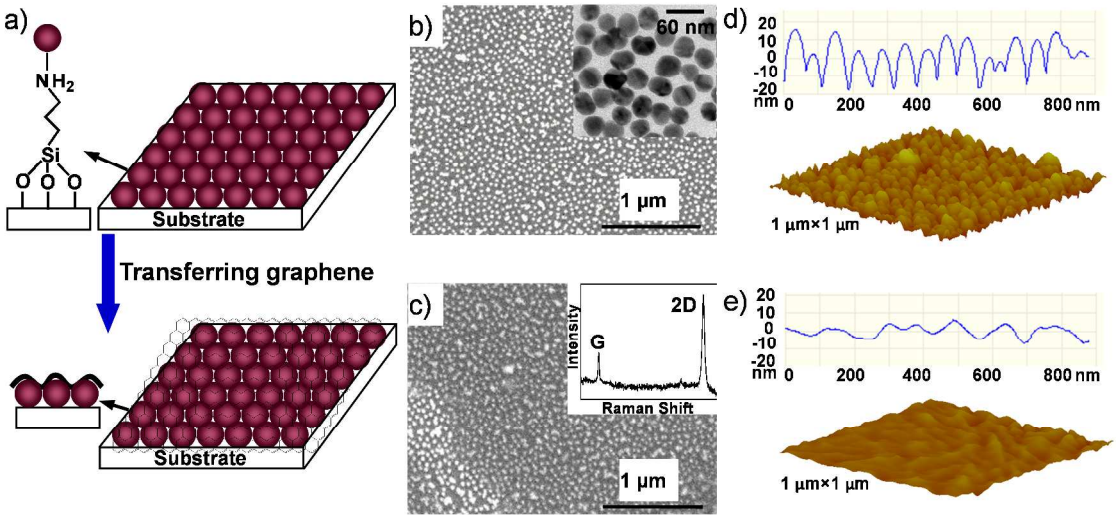

Fig. 1 a) Schematic of the fabrication of graphene-Au NPs hybrid films. b) SEM image of ~30 nm Au NPs deposited on Si with density of 343 No./μm^2. Inset shows the TEM image of Au NPs. c) SEM image of monolayer graphene-coated Au NPs. The dark area is covered by monolayer graphene, as confirmed by the Raman spectrum in the inset. AFM images of Au NPs d) without and e) with monolayer graphene transferred. The line profiles in d) and e) were randomly taken from each AFM scan, indicating the different roughness of two samples.

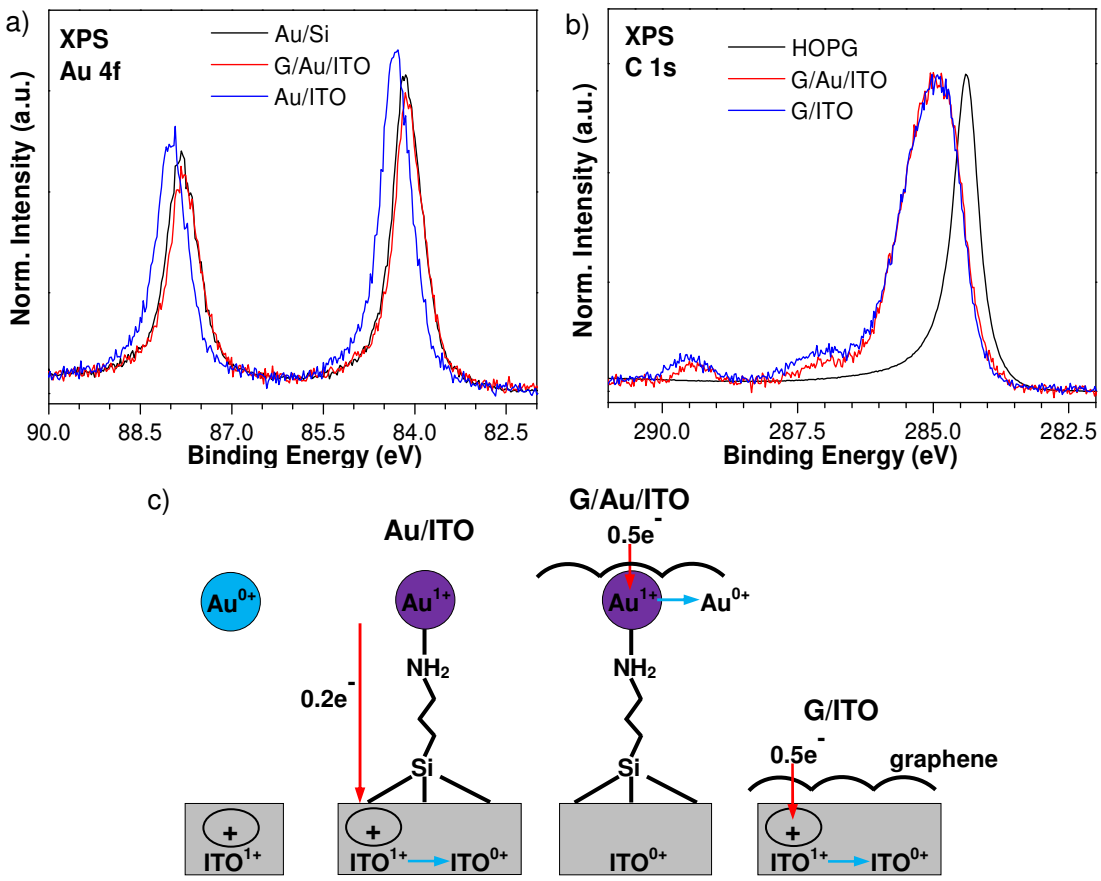

Fig. 2 a) XPS Au 4f spectra of thick Au film on a Si substrate and ~30 nm Au NPs on ITO substrates with or without monolayer graphene coated. b) XPS C 1s spectra of HOPG and graphene on ITO substrates with or without ~30 nm Au NPs underneath. c) Schematic showing the charge transfers from Au NPs to ITO, from graphene to Au NPs, and from graphene to ITO, respectively, for different XPS samples.

The topography of graphene-Au NPs hybrid films was checked with AFM (Fig. 1e), with that of bare Au NPs as reference (Fig. 1d). The AFM image in Fig. 1e reveals the uniform surface morphology after graphene was coated on the Au NPs, leading to a smaller roughness (arithmetic average deviation) of 3.25 nm compared with that of 8.35 nm for bare Au NPs. Furthermore, we can see that the graphene bridges dispersive Au NPs with no significant breakage on the scale scanned and deforms itself to conform to the geometry of Au NPs. Such a close contact between graphene and the underlying Au nanostructures is expected to improve the electromagnetic hot spots at the interface between graphene and Au, which may largely contribute to the enhanced Raman signals of adsorbates on the hybrid films, as discussed below.

To further explore the interface between graphene and Au NPs, high-resolution X-ray photoelectron spectroscopy (XPS) with a synchrotron photon source has been done. To do XPS measurements, conductive ITO has been selected as substrates for depositing Au NPs, with or without graphene coating. The fabrication procedures were kept exactly same. Fig. 2a shows the Au 4f core-level spectra of Au/ITO and G/Au/ITO as compared with that of a thick Au film on a Si substrate. The binding energies (BEs) of Au $4f_{7/2}$ and $4f_{5/2}$ states in the thick Au/Si measured are 84.1 and 87.8 eV, respectively, in a good agreement with Au metal measurement.[32] With respect to metallic Au^0 state in think Au film, 30 nm Au NPs on ITO behave an up-shift in the BEs of $4f_{7/2}$ and $4f_{5/2}$ states by 0.2 eV. The shift is ascribed to the -NH_2 end groups bonded to the surface of Au NPs (Fig. 2c), consistent with the result of Au nanocrystals with amine groups.[33] After being coated with graphene, the XPS spectrum of graphene-coated Au NPs has the same peak width and BEs as those from Au/Si; the BE peaks show a down-shift compared to that of bare Au NPs without graphene. As the work functions of Au (~5.31 eV) and graphene (~4.48 eV) are different,[34] the electron transfer from graphene to Au NPs may occur for the Fermi energy alignment. Fig. 2b shows C 1s spectra of G/Au/ITO, G/ITO, and standard HOPG sample. The chemical environment of HOPG is considered as sp^2-hybridized carbon, showing an intensive peak at a BE of 284.4 eV. The C 1s XPS peak of G/ITO shows a broadened width and an upshift of 0.5 eV relative to that of HOPG. Although the chemical and lattice structure of graphene is analogous to the single layer HOPG, it is reasonable to see the electron transfer response when the delocalized π electrons in the honeycomb structure of graphene are in contact with the oxygen vacancy in the ITO substrate.[35,36] The nearly same C1s peak features in G/Au/ITO can be explained by the good contact between graphene and Au NPs, which provided an efficient electron transfer path from graphene to Au, as supported by the good morphological conformance in AFM results. The high BE side and the shoulders at BEs of 287.0 and 289.5 eV result from the surface carbon adsorption on ITO; for the reason, they are almost equal in G/Au/ITO and G/ITO while the probing depth of X-ray beam is larger than the thickness of a monolayer graphene. As schematically described in Fig. 2c, whereas the π electrons of graphene layer are driven to transfer

into the oxidized Au state of G/Au/ITO, the consequence of ~0.5 eV upshift of C 1s state is addressed in the upper monolayer graphene. Such an up-shift in C 1s peak compared to the case in HOPG is consistent to the down-shift in the Au 4f state of graphene-Au NPs on ITO, confirming the electron transfer from graphene to Au NPs.

3.2 Optical properties of graphene-Au nanoparticles hybrid films

was transferred, the addition layers of graphene coating did not change the transmittances much as the first layer. In fact, for the second, third or fourth transfer, the decrease in the transmittance linearly depends on the number of graphene layers and the resonance wavelength shows only a slight change, as shown in Fig. 3b and S3†. Furthermore, when the size of Au NPs is fixed, the transmittance at plasmonic resonance for the hybrid films consisting of monolayer

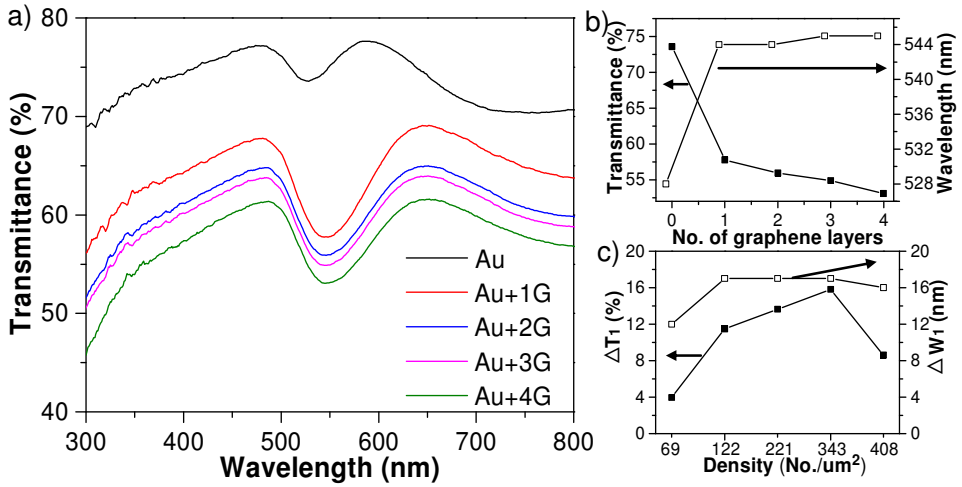

Fig. 3 a) Transmission spectra of ~30 nm Au NPs with density of ~343 No./μm^2 deposited on quartz substrates before and after different numbers of graphene layers were coated. b) Transmittance and wavelength at plasmonic resonance as function of number of graphene layers coated on ~30 nm Au NPs with density of ~343 No./μm^2. c) Absolute transmittance change and resonance dip wavelength shift compared to bare Au NPs as function of cover density for the hybrid films consisting of monolayer graphene and ~30 nm Au NPs.

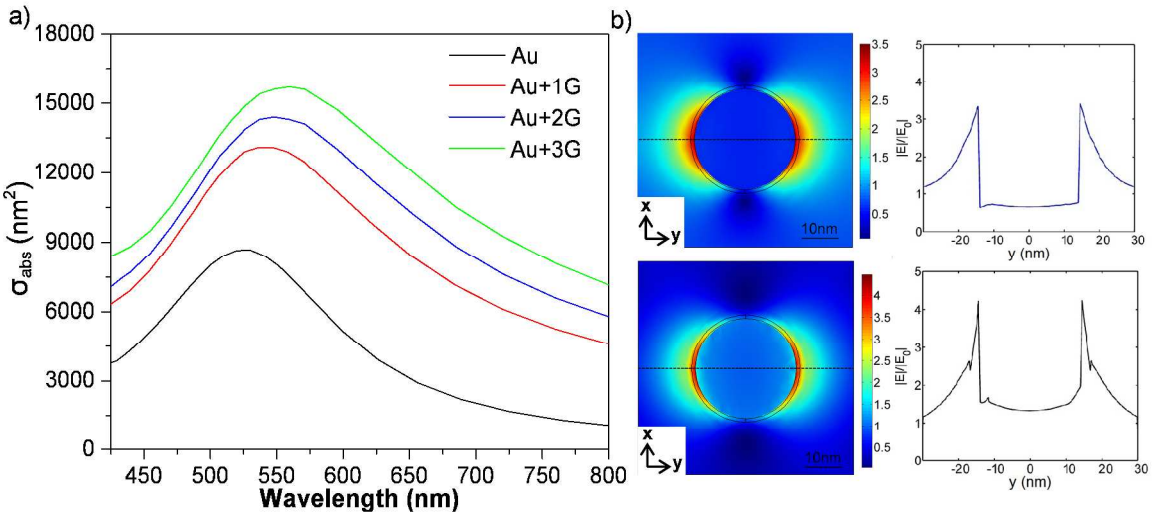

Fig. 4 a) FEM simulated absorption cross-section for ~30 nm Au NPs without graphene (black lines) or with one (red lines), two (blue lines) and three (green lines) layers of graphene transferred on Au NPs. b) Simulated electric field distributions and corresponding line profiles along the y direction (dotted line) for Au NPs (top) without and (below) with monolayer graphene coated.

The optical transmission of Au NPs on quartz substrates has been significantly modulated by the graphene layers covered. As can be seen from Fig. 3a, deepening, broadening and red-shift of the plasmonic resonance dip was observed upon the coating of monolayer graphene, accompanied by a large decrease in the absolute transmittance of about 15.8%. Such a transmittance decrease is much higher than the typical 2.3% transmittance loss for monolayer graphene in the same wavelength range. Interestingly, once the first layer of graphene graphene shows a monotonous increase with the coverage density of Au NPs of up to ~343 No./μm^2, then a decrease for the higher density of ~408 No./μm^2 (Fig. 3c and S3†). The decreased transmittance for the very high density of Au NPs may be attributed to the aggregation of NPs, as shown in Fig. S3d† and Table S1†. The resonance wavelength shift upon graphene coverage was studied as well. For the lowest density Au sample, the transmission dip experiences a smaller wavelength shift (~12 nm) than the others (~17 nm) (Fig. 3c

and S3†), indicating that the interaction between light and the hybrid films is heavily affected by the contact areas between graphene and plasmonic Au NPs. In addition, Fig. S4† shows that the trend of the decrease in the transmittance and the resonance wavelength red-shift remains similar for the graphene-coated Au NPs with the average size of nanoparticles of ~15 nm and ~45 nm, respectively.

As we can see below, the modulated and suppressed optical transmittance of graphene-Au NPs hybrid films can be explained by the changes in the surroundings dielectric function and refractive index of Au plasmonic nanoparticles.[37] Graphene effectively mimics a dielectric material in the visible and near-infrared wavelength ranges.[38] Similar to the case where a plasmonic nanostructure embedded in the medium with a higher refractive index,[37,39] the red-shift in the plasmonic resonance and suppressed transmittance in the graphene-Au NPs hybrid films in this work are attributed to the presence of graphene and the graphene Ohmic loss.[25] As the experimental results show, the coupling between charge carriers in first layer of graphene and the surface plasmons of Au NPs is much stronger than the localized surface plasmon resonance (LSPR) of individual nanoparticles. Such a hybrid film therefore provides a platform for the chemical sensing, e.g. by enhanced Raman scattering as described below. As we can see from the following discussion, the reason for the sensitivity enhancement lies in the facts that LSPR is coupled by a diffractive wave propagating along the surface of the sample, and that the wave spread is mainly affected by conductivity and dielectric permittivity of graphene.[40]

Fig. 4a shows the finite element simulated absorption cross sections as the function of incident wavelength for Au NPs on a glass substrate without graphene or with one, two and three layers of 0.5 nm-thick graphene. The calculated plasmonic resonance wavelength is approximately 530 nm for bare Au NPs on the glass substrate, matching well to the experimental observations. Coating a monolayer graphene on the Au hemisphere results in a dampening of the plasmonic resonance and thus leads to a resonance shift towards longer wavelengths and a broadening of the resonance peak as well. The increased absorbance near the resonance wavelength is caused by the enhanced light-matter interaction, indicated by the increased electric field intensity of plasmonic resonance as shown in Fig. 4b and with more details in Fig. S5†. Fig. 4b shows that the maximum electric field intensity around Au NPs coated with monolayer graphene is increased to approximately 4.4 from the value of 3.5 for the bare Au NPs, corresponding to a 19.36-fold enhancement of the optical absorption, compared to the 12.25-fold enhancement for bare Au NPs as estimated from Formula (1). Since the reflection of graphene can be neglected for a normal incidence,[31] the calculated absorption cross section thus provides a qualitative explanation for the decrease in transmittance for graphene-Au NPs hybrid films observed in experiments. In addition, by comparing the electromagnetic field distribution of the Au NPs before and after graphene coating, we can see from Fig. 4b that the electromagnetic field is more confined in a narrower region for the graphene-Au NPs hybrids, due to the coupling of graphene and plasmonic Au NPs.

3.3 SERS properties of the graphene-Au nanoparticles hybrid films

It is well-known that noble metals such as Ag and Au nanocrystals can serve as excellent substrates for SERS based on the enhanced local electromagnetic field due to the surface plasmons. As a substrate potentially useful for detecting Raman signals of molecules, graphene not only had capability of adsorbing molecule and quenching fluorescence background, but also could demonstrate chemical enhancement based on charge transfer to enhance the Raman scattering of the molecules.[21] In this work, R6G was chosen to probe the SERS effect of the graphene-Au NPs hybrid films. Fig. 5a shows the average Raman intensities (collected from 30 spectra taken from random spots on each film) of 2 μL R6G ethanol solution with various molecular concentrations immobilized on monolayer graphene-Au NPs hybrid films. The Raman peaks at 612 cm^{-1}, 774 cm^{-1}, 1186 cm^{-1}, 1360 cm^{-1}, 1506 cm^{-1}, and 1648 cm^{-1} are in good agreement with previous reports for R6G.[26]

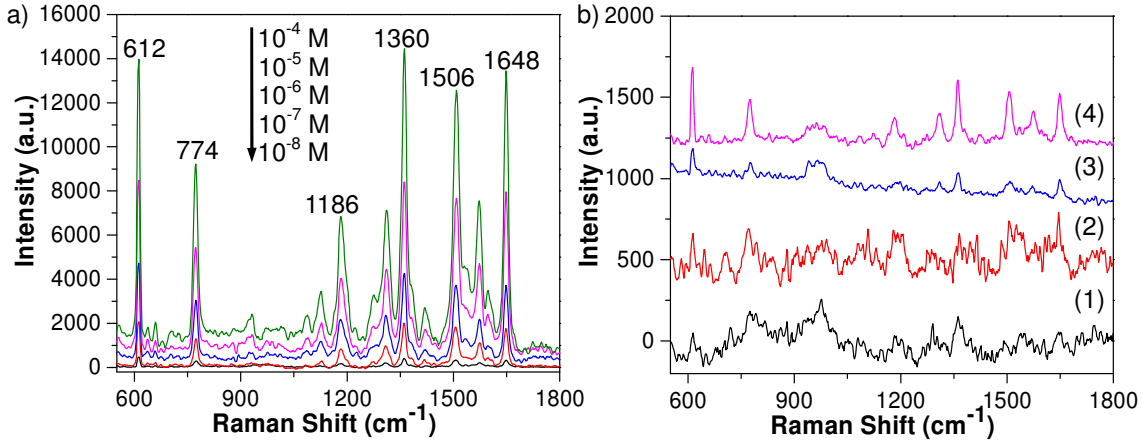

Fig. 5 a) SERS spectra of R6G with varied concentrations on monolayer graphene-Au NPs hybrid films. b) SERS spectra of 10^{-2} M R6G on quartz (curve 1), 10^{-3} M on graphene/quartz (curve 2), 10^{-7} M on Au NPs/quartz (curve 3), and 10^{-8} M on the monolayer graphene-Au NPs hybrid films (curve 4). The baseline has been subtracted from each spectrum.

The Raman signal was still visible for a R6G concentration of as low as 10^{-8} M. The SERS enhancement factors (EF) for R6G on the graphene-Au NPs hybrid films were calculated according to the equation EF= $(I_{SERS}/I_{bulk})(N_{bulk}/N_{surface})$, where

I_{SERS} and I_{bulk} are the 612 cm^{-1} peak intensities obtained from 10^{-8} M R6G on the hybrid films and from 10^{-2} M R6G obtained on a quartz substrate (Fig. 5b), respectively. N_{SERS} and N_{bulk} are the numbers of R6G molecules excited by the laser beam on the hybrid films and quartz substrate, respectively. An EF of about ~10^7 was calculated for the graphene-Au NPs hybrid films with Au NPs cover density of ~343 No./μm^2. Compared to the bare Au NPs film (Fig. 5 and S6†), the graphene-Au NPs hybrid film shows an enhancement of 14-fold in EF values. The enhancement factors for the bare Au NPs samples and graphene coated Au NPs hybrids have been calculated for different cover densities of Au NPs and shown in Fig. S7†.

Such a graphene related enhancement could be due to graphene-induced fluorescence quenching, adsorption enrichment, chemical enhancement and electromagnetism enhancement from the coupling of charge carriers in graphene and surface plasmons in Au NPs. It has been reported that monolayer graphene facilitates charge transfer between graphene and probe molecules, resulting in a vibration-mode dependent enhancement of 2-17 times.[41] Based on graphene covered Au nanovoid arrays[25] and Au nano-pyramids[26] fabricated with template technology, SERS enhancement factors of 1.8 and 10 were attributed to the introduction of graphene when being used to sense R6G molecules. In SERS, the enhancement factor could be estimated from the localized electromagnetic enhancement by

$$\gamma \approx \frac{|E_t|^4}{|E_i|^4}, \quad (2)$$

where E_i is the incident field intensity and E_t is the field intensity at the location of molecules detected. Fig. S8† shows the simulated electrical field distributions around Au NPs with or without monolayer graphene transferred at the Raman laser wavelength of 532 nm (slightly different from plasmonic resonance frequency of Au). With graphene coating, the maximum enhancement of electrical field intensity is increased to 4.2, corresponding to an electromagnetic enhancement of about 311 for SERS. In contrast, the maximum enhancement of electrical field intensity and estimated electromagnetic enhancement are 3.7 and 187 for bare Au NPs deposited on the quartz substrate.

Additionally, we found that graphene makes the SERS detection more stable. Due to the large area completeness and chemical stability of graphene, the graphene coating in the hybrid films may keep most of R6G molecules from directly contacting with Au NPs, thus preventing R6G molecules from photocarbonization.[42,43] On the other hand, in conventional SERS experiments especially for dyes, the photobleaching of the Raman probes induced by the laser may lead to uncontrollable variations of the SERS spectra with acquisition time and laser power.[21] As shown in Fig. 6, time-resolved Raman spectroscopy was carried out to compare the SERS detection stability of the bare Au NPs and graphene-coated Au

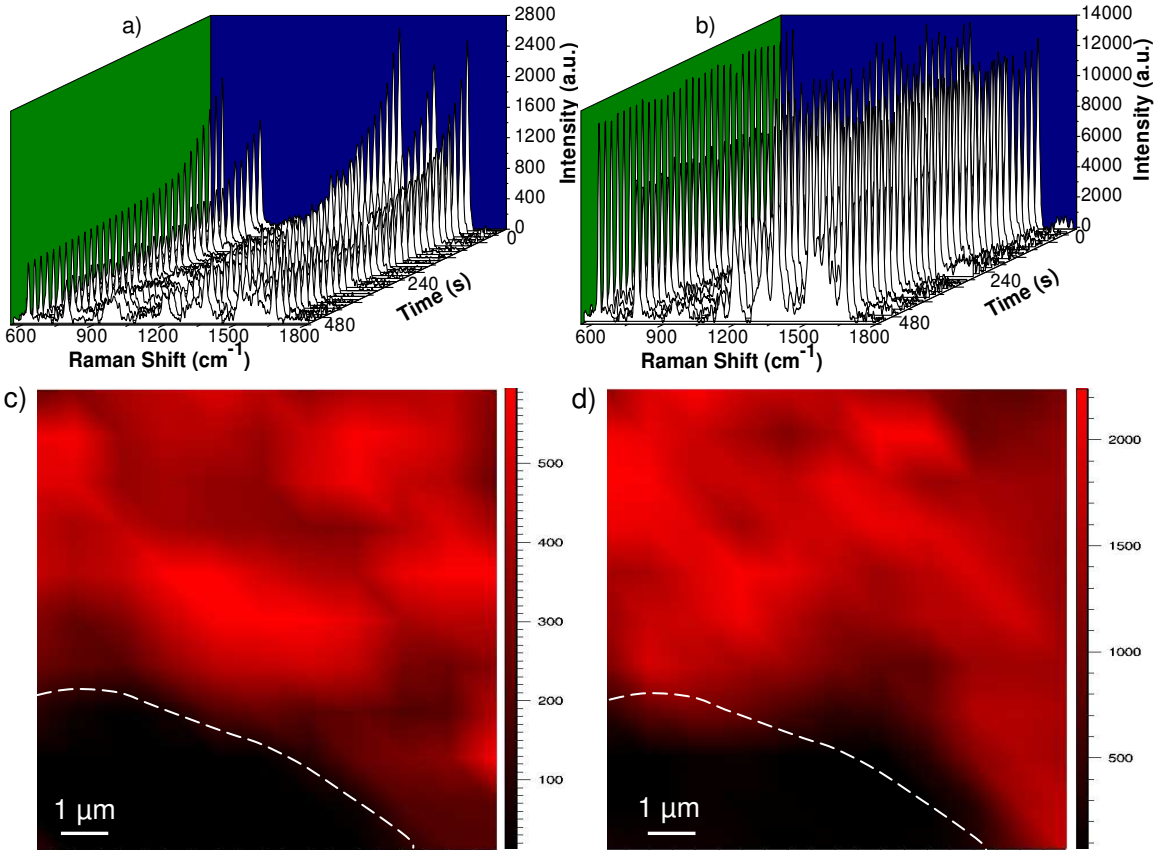

Fig. 6 Evolution of SERS signals from 10^{-4} M R6G on a) Au NPs films and b) graphene-Au NPs hybrid films, respectively (the data were collected at an interval of 20 s). Spatial resolved Raman intensity mapping of c) graphene G peak and d) 612 cm^{-1} peak of 10^{-7} M R6G on graphene-Au NPs hybrid films with the boundary of graphene sheet indicated by the dash line. The region below the dash line is bare Au NPs without graphene coverage. The boundary was determined according to the optical picture recorded by Renishaw inVia Raman Microscope.

NPs on the same substrate. It can be seen that the SERS signals intensity of R6G on the bare Au NPs decayed quickly during a 480 s-long measurement while signals of R6G on graphene-Au NPs hybrids remain much more stable. This stabilization effect could be related to the metal-molecule isolation induced by surface passivation effect of graphene and/or the formation of a graphene-molecule complex (especially aromatic molecules) through π-π interactions.[22] Furthermore, the high thermal conductivity of graphene may also contribute to the enhanced stability by dissipating the heat more efficiently. In fact it has been found that the morphology of the metal film changes after being exposed to a relatively large laser power while it keeps stable with graphene covered.[43] We also carried out Raman studies of R6G with different concentrations (Fig. S9†) on the same graphene-Au NPs hybrid film substrate after it was kept for half a year in our lab. The Raman intensity of R6G only showed a little decrease (Fig. S10†). Thus the graphene-Au NPs hybrid films fabricated by the simple and cost-effective self-assembly method are able to reach the stability requirements in practical applications.

The high uniformity and reproducibility of SERS signals are essential for its practical application especially when the concentration and/or the amount of adsorbates are very low. As we can see from Fig. S7† and Fig. S11†, while the SERS sensitivity for bare Au NPs is similar for different cover densities, the uniformity is improved with the cover density till the value of ~343 No./μm^2. A higher cover density of ~408 No./μm^2 leads to deteriorated uniformity due to the higher degree of aggregation (Fig. S11†). The homogeneity of SERS signals on the hybrids films with the cover density of ~343 No./μm^2 was further investigated by performing a spatial resolved Raman intensity mapping across a graphene boundary (indicated by the dash line in Fig. 6c). The region below the dash line is bare Au NPs without graphene coverage. As shown in Fig. 6c and 6d, the SERS intensity mapping of R6G shows a high consistency to the Raman G peak mapping of graphene. Such a result clearly indicates that the presence of graphene is essential to the enhanced SERS detection ability for R6G molecules. Also, the area covered with graphene (above the dash line) shows a highly homogeneous adsorption for R6G, further making the graphene based SERS detection attractive in practical applications.

4. Conclusions

In summary, we have demonstrated enhanced the light-graphene interaction by fabricating graphene-Au NPs hybrid films and investigating their optical properties. A large decrease in transmittance, red-shift, broadening of the plasmonic resonance was observed when a monolayer graphene was transferred on top of Au NPs. The effects of size and density of Au NPs, and number of graphene layers were investigated. The experimental observations were explained by finite element numerical simulations. In addition, we have demonstrated that the hybrid films are high-performance candidates for SERS applications due to the combined effects of the electromagnetism enhancement activity at the graphene and Au interface, and the surface enrichment, fluorescence quencher and additional chemical enhancement of graphene. Using R6G molecules as probes, we obtained the SERS enhancement factors of up to ~10^7 on graphene-Au NPs hybrid films, with a stable and homogenous response. The simple and rapid SERS sensor reported here may open up new opportunities in developing the applications of graphene in biomedical diagnostics, analytical chemistry, as well as biological sensing and imaging.

Acknowledgements

The authors thank support from China Government 1000Plan Talent Program, China MOE NCET Program and Natural Science Foundation of China (51322204). C.-H. Chuang acknowledges the National Science Council of Taiwan for financial support under Contract No. NSC 102-2112-M-032-001.

Notes and references

[a] Department of Materials Science and Engineering & CAS Key Laboratory of Materials for Energy Conversion, University of Science and Technology of China, 96 Jin Zhai Rd, Hefei 230026, China.
*Corresponding author, E-mail: zhuyanwu@ustc.edu.cn
[b] Wuxi Graphene Technologies Co., Ltd, 311 Yanxin Rd, Wuxi 214174, China & Jiangnan Graphene Research Institute, 6 Xiangyun Rd, Changzhou 213149, China.
[c] National Synchrotron Radiation Research Center, Hsinchu 300, Taiwan.
[d] Department of Physics, Tamkang University, New Taipei City 25137, Taiwan.

† Electronic Supplementary Information (ESI) available: Additional information including UV-vis absorption spectra and TEM images of Au NPs with different sizes, optical image and transmission spectra of monolayer graphene, SEM image of Au NPs covered with a large-area monolayer graphene, transmission spectra of Au NPs with different size or cover density before and after different layers graphene coated, Raman spectra of R6G on Au NPs with different concentrations and simulated electric field distributions at the laser wavelength for Au NPs with or without monolayer graphene covered. See DOI: 10.1039/b000000x/

1 K. S. Novoselov, A. K. Geim, S. V. Morozov, D. Jiang, Y. Zhang, S. V. Dubonos, I. V. Grigorieva and A. A. Firsov, *Science*, 2004 , **306**, 666.
2 A. N. Grigorenko, M. Polini and K. S. Novoselov, *Nat. Photonics*, 2012, **6**, 749.
3 R. R. Nair, P. Blake, A. N. Grigorenko, K. S. Novoselov, T. J. Booth, T. Stauber, N. M. R. Peres and A. K. Geim, *Science*, 2008, **320**, 1308.
4 A. H. Castro Neto, F. Guinea, N. M. R. Peres, K. S. Novoselov and A. K. Geim, *Rev. Mod. Phys.*, 2009, **81**, 109.
5 F. Bonaccorso, Z. Sun, T. Hasan and A. C. Ferrari, *Nat. Photonics,* 2010, **4**, 611.
6 A. Pospischil, M. Humer, M. M. Furchi, D. Bachmann, R. Guider, T. Fromherz and T. Mueller, *Nat. Photonics,* 2013, **7**, 892.
7 H. Chang, Z. Sun, M. Saito, Q. Yuan, H. Zhang, J. Li, Z. Wang, T. Fujita, F. Ding, Z. Zheng, F. Yan, H. Wu, M. Chen and Y. Ikuhara, *ACS nano*, 2013, **7**, 6310.
8 E. O. Polat and C. Kocabas, *Nano Lett.*, 2013, **13**, 5851.
9 J. B. Bult, R. Crisp, C. L. Perkins and J. L. Blackburn, *ACS nano*, 2013, **7**, 7251.
10 J. Liu, N. Liu, J. Li, X. Li and J. Huang, *Appl. Phys. Lett.*, 2012, **101**, 052104.

11 M. Engel, M. Steiner, A. Lombardo, A. C. Ferrari, H. V. Lo hneysen, P. Avouris and R. Krupke, *Nat. Commun.*, 2012, **3**, 906.
12 T. Mueller, F. Xia and P. Avouris, *Nat. Photonics*, 2010, **4**, 297.
13 X. Huang, I. H. El-Sayed, W. Qian and M. A. El-Sayed, *J. Am. Chem. Soc.*, 2006, **128**, 2115.
14 P. K. Jain, X. Huang, I. H. El-Sayed and M. A. El-Sayed, *Acc. Chem. Res.*, 2008, **41**, 1578.
15 S. Nie and S. R. Emory, *Science*, 1997, **275**, 1102.
16 J. N. Anker, W. P. Hall, O. Lyandres, N. C. Shah, J. Zhao and R. P. Van Duyne, *Nat. Mater.*, 2008, **7**, 442.
17 I. Chourpa, F. H. Lei, P. Dubois, M. Manfait and G. D. Sockalingum, *Chem. Soc. Rev.*, 2008, **37**, 993.
18 T. J. Echtermeyer, L. Britnell, P. K. Jasnos, A. Lombardo, R. V. Gorbachev, A. N. Grigorenko, A. K. Geim, A. C. Ferrari and K. S. Novoselov, *Nat. Commun.*, 2011, **2**, 458.
19 W. Ren, Y. Fang and E. Wang, *ACS nano*, 2011, **5**, 6425.
20 S. He, K. K. Liu, S. Su, J. Yan, X. Mao, D. Wang, Y. He, L. J. Li, S. Song and C. Fan, *Anal. Chem.*, 2012, **84**, 4622.
21 W. Xu, N. Mao and J. Zhang, *Small*, 2013, **9**, 1206.
22 W. Xu, J. Xiao, Y. Chen, Y. Chen, X. Ling and J. Zhang, *Adv. Mater.*, 2013, **25**, 928.
23 G. Lu, H. Li, C. Liusman, Z. Yin, S. Wu and H. Zhang, *Chem. Sci.*, 2011, **2**, 1817.
24 Z. Zhang, F. Xu, W. Yang, M. Guo, X. Wang, B. Zhang and J. Tang, *Chem. Commun.*, 2011, **47**, 6440.
25 X. Zhu, L. Shi, M. S. Schmidt, A. Boisen, O. Hansen, J. Zi, S. Xiao and N. A. Mortensen, *Nano Lett.*, DOI:10.1021/nl402120t.
26 P. Wang, O. Liang, W. Zhang, T. Schroeder and Y. H. Xie, *Adv. Mater.*, 2013, **25**, 4918.
27 Y. Du, R. Liu, B. Liu, S. Wang, M.-Y. Han and Z. Zhang, *Anal. Chem.*, 2013, **85**, 3160.
28 X. Li, W. Cai, J. An, S. Kim, J. Nah, D. Yang, R. Piner, A. Velamakanni, I. Jung, E. Tutuc, S. K. Banerjee, L. Colombo and R. S. Ruoff, *Science*, 2009, **324**, 1312.
29 S. Bae, H. Kim, Y. Lee, X. Xu, J.-S. Park, Y. Zheng, J. Balakrishnan, T. Lei, H. R. Kim and Y. I. Song, *Nat. Nanotechnol.*, 2010, **5**, 574.
30 Edward D. Palik. Handbook of opical contants of solids, Academic, New York, USA **1985**.
31 M. Bruna and S. Borini, *Appl. Phys. Lett.*, 2009, **94**, 031901.
32 C. J. Powell, N. E. Erickson and T. Jach, *J. Vac. Sci. Technol.*, 1982, **20**, 625.
33 D. V. Leff, L. Brandt and R. Heath, *Langmuir*, 1996, **12**, 4723.
34 J. Li, C. Liu and Y. Liu, *J. Mater. Chem.*, 2012, **22**, 8426.
35 H. Ishii, K. Sugiyama, E. Ito and K. Seki, *Adv. Mater.*, 1999, **11**, 605.
36 K. L. Purvis, G. Lu, J. Schwartz and S. L. Bernasek, *J. Am. Chem. Soc.*, 2000, **122**, 1808.
37 T. Okamoto, I. Yamaguchi and T. Kobayashi, *Optics Lett.*, 2000, **25**, 372.
38 M. Jablan, H. Buljan and M. Solja cíc, *Phys. Rev. B*, 2009, **80** ,245435.
39 X. Yu, L. Shi, D. Han, J. Zi and P. V. Braun, *Adv. Funct. Mater.*, 2010, **20**, 1910.
40 V. G. Kravets, F. Schedin, R. Jalil, L. Britnell, K. S. Novoselov and A. N. Grigorenko, *J. Phys. Chem. C*, 2012, **116**, 3882.
41 X. Ling, L. M. Xie, Y. Fang, H. Xu, H. L. Zhang, J. Kong, M. S. Dresselhaus, J. Zhang and Z. F. Liu, *Nano Lett.*, 2010, **10**, 553.
42 J. F. Li, Y. F. Huang, Y. Ding, Z. L. Yang, S. B. Li, X. S. Zhou, F. R. Fan, W. Zhang, Z. Y. Zhou, D. Y. Wu, B. Ren, Z. L. Wang and Z. Q. Tian, *Nature*, 2010, **464**, 392.
43 W. Xu, X. Ling, J. Xiao, M. S. Dresselhaus, J. Kong, H. Xu, Z. Liu and J. Zhang, *Proc. Natl. Acad. Sci. USA*, 2012, **109**, 9281.

Table of Content

We demonstrate enhanced light-matter interactions in graphene-Au nanoparticles hybrid films and the application for high quality SERS detection.